Letter

Inverse Photoemission Spectroscopy of Coinage Metal Corroles: Comparison with Solution-Phase Electrochemistry

Published as part of ACS Organic & Inorganic Au virtual special issue "Electrochemical Explorations in Organic and Inorganic Chemistry".

Luca Giovanelli,* Younal Ksari, Hela Mrezguia, Eric Salomon, Marco Minissale, Abraham B. Alemayehu, and Abhik Ghosh*

Read Online

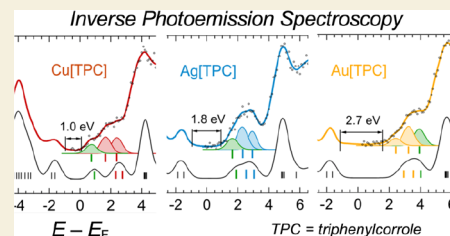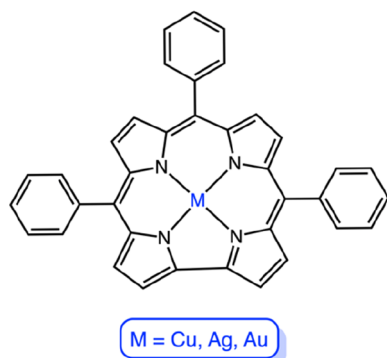ACCESS | Metrics & More | Article Recommendations | Supporting Information

ABSTRACT: A combined direct and inverse photoemission study of coinage metal corroles suggests that the latter technique, in favorable cases, can provide some additional information relative to electrochemical measurements. Thus, whereas inverse photoemission spectroscopy (IPES) provides relative electron affinities for electron addition to different unoccupied orbitals, electrochemical reduction potentials shed light on the energetics of *successive* electron additions. While all three coinage metal triphenylcorrole (TPC) complexes exhibit similar ionization potentials, they exhibit dramatically different inverse photoemission spectra. For Cu[TPC], the lowest-energy IPES feature (0.74 eV) is found to be exceedingly close

Inverse Photoemission Spectroscopy

to the Fermi level; it is significantly higher for Ag[TPC] (1.65 eV) and much higher for Au[TPC] (2.40 eV). These differences qualitatively mirror those observed for electrochemical reduction potentials and are related to a partially metal-centered LUMO in the case of Cu- and Ag[TPC] and a fully corrole-based LUMO in the case of Au[TPC]; the latter orbital corresponds to the LUMO +1 in the case of Ag[TPC].

KEYWORDS: photoemission, photoelectron, inverse photoemission, corrole, copper, silver, gold

The last quarter-century has seen corroles catapulted from relative obscurity to the forefront of chemical and

Scheme 1. Complexes Studied in This Work: M[TPC] (M = Cu, Ag, Au)

M = Cu, Ag, Au

materials sciences and wide-ranging medical and technological applications.[1,2] Redox-active metallocorroles, thus, are widely used as catalysts, especially as electro- and photo catalysts.[3−6] Redox-innocent metallocorroles, especially those involving 5d transition elements, hold particular promise for medicine, perhaps most notably as triplet photosensitizers for oxygen

sensing and photodynamic and related therapies.[7−11] The new applications have built directly on an ever-deepening understanding of metallocorroles' electronic structure, at the center of which, arguably, lies the phenomenon of ligand noninnocence.[12−14] Noninnocent ligands, it may be recalled, do not allow a straightforward determination of the oxidation state of a coordinated metal.[15,16] A tricky concept, the phenomenon can nonetheless be probed by a battery of physical and quantum chemical methods; very recently, the phenomenon has even been quantified.[17,18] Presented herein is a first exploration of the potential application of inverse photoemission spectroscopy (IPES) to corrole derivatives.

Inverse photoemission spectroscopy,[19−22] the time-reversed counterpart of direct photoemission spectroscopy[23−26] (also called photoelectron spectroscopy, PES), plays an important role in study of the unoccupied states of materials. In a typical experiment, a monochromatic electron beam impinges on a surface, resulting in the emission of photons whose energies
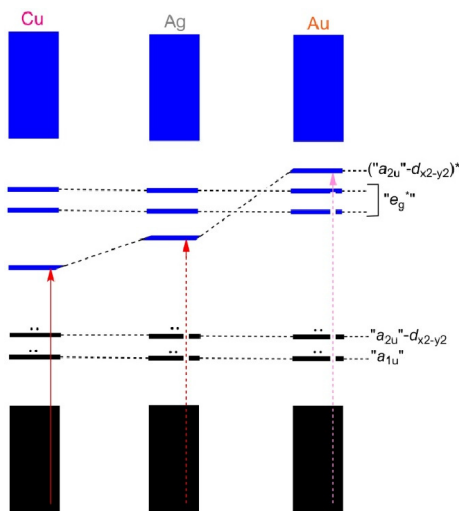
A

Figure 1. Schematic energy level diagram for of Cu-, Ag-, and Au-TPC complexes. Occupied and unoccupied MOs are indicated in black and blue, respectively. Note that the HOMO energy levels are similar. However, the LUMO energy levels vary across the three complexes as a result of varying levels of interaction between the corrole's π-HOMO and the formally empty metal (d_{x2-y2}) orbital. Reproduced from ref 13. Copyright 2017 American Chemical Society.

are analyzed. The incident electrons couple to unoccupied states of the material and decay to lower states via both radiative and nonradiative pathways and the energies of the radiated photons provides a map of the unoccupied state architecture. In a simpler implementation of the experiment, the so-called isochromat mode, the energy of the incident electrons (E_i) is varied, while photons are detected at a fixed energy ($h\nu$), with a narrow bandpass on the order of a 100 meV. Regardless of the implementation, the energy of the final state (E_f) is given by $E_f = E_i - h\nu$. Together, direct (UPS) and inverse photoemission spectroscopy (IPES) provide a picture of the band structure of a material.[27]

Unlike PES, IPES has enjoyed relatively few applications in molecular chemistry.[28−34] Simpler tools such as electrochemistry and optical spectroscopy have typically afforded the necessary insight into molecular excited states. That said, IPES does provide unique insight. While electrochemical reduction potentials afford information on the energetics of *successive* reductions (i.e., electron additions), IPES probes the energetics of individual unoccupied molecular orbitals (MOs). To determine the potential usefulness of IPES in a coordination chemistry context, we carried out a direct and inverse photoemission study of coinage metal *meso*-triphenyl-corrole complexes, M[TPC] (M = Cu, Ag, Au; Scheme 1). The solution-phase reduction potentials of the three complexes vary from −0.20 V for Cu[TPC] through −0.86 V for Ag[TPC] to −1.38 V for Au[TPC] (all vs the saturated calomel electrode), indicating dramatically rising energies of the lowest unoccupied MO (LUMO) from Cu through Ag to Au.[35−37] The electronic structures of the complexes also vary from a noninnocent $Cu^{II}-Cor^{\bullet 2-}$ description for Cu-[TPC][38−44] to an essentially innocent $M^{III}-Cor^{3-}$ description for Ag[TPC][37] and Au[TPC];[45−53] these differences are schematically summarized in Figure 1. We shall see that the IPES-derived picture of unoccupied states is eminently consistent with that derived from electrochemistry[35−37,54] and other spectroscopic methods (such as X-ray absorption
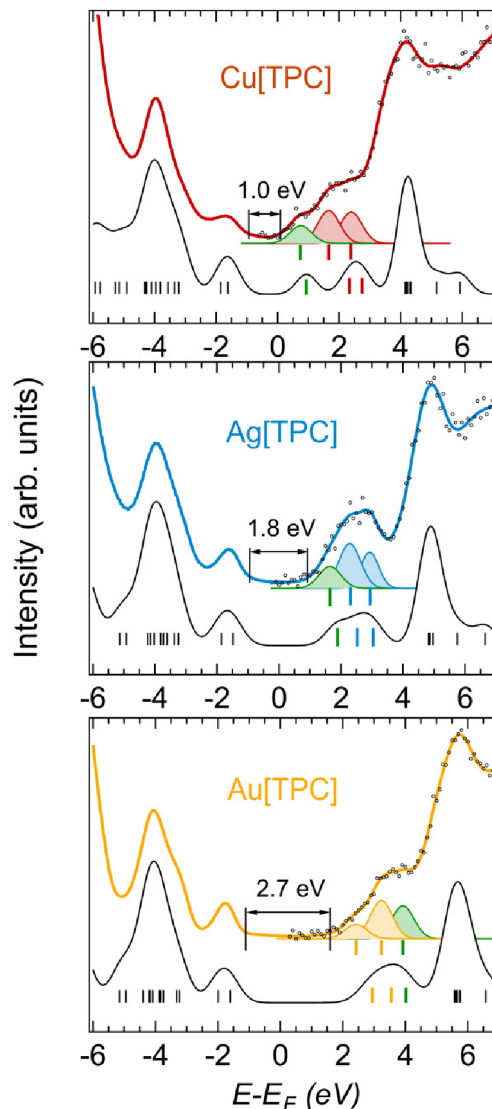

Figure 2. Experimental (upper curves) and calculated (lower curves) density of states (DOS) for the three M-TPC. Experimental curves are composed of UPS spectra (negative energies) measuring the occupied DOS up to the Fermi level (zero energy) and IPES spectra measuring the unoccupied DOS. For IPES, colored lines are the result of the fitting procedure to the experimental data (markers). All spectra are referenced to the Fermi level (E_F). For each set of spectra, the three colored Gaussian curves correspond to the lowest unoccupied MO (LUMO), LUMO+1, and LUMO+2, resulting from the least-squares fitting of the IPES spectra. Their energy positions are highlighted by vertical bars. The experimental energy gap (E_g) is indicated. Its value is determined as the energy difference between the HOMO and LUMO leading-edges' intersections with the baseline (not shown).

spectroscopy[55,56]). Moreover, combining the UPS and IPES data gives access to the solid-state band gap (E_g),[57] a value that can be compared to the electrochemical HOMO−LUMO gap (E_{ox-red}), which is the difference between solution-phase oxidation and reduction potentials obtained from electrochemical measurements.[58]

Herein, all samples were prepared under ultrahigh vacuum (UHV) conditions. The M[TPC] samples were sublimed from an alumina crucible heated by a tungsten filament. For Cu- and Au[TPC], a sublimation temperature of 250 °C was used,

Table 1. IPES Peak Positions Relative to the Fermi Level, UPS- and IPES-Derived Band Gaps (E_g), and Electrochemical HOMO−LUMO Gaps (E_{ox-red})^a

Compound	Peak a	Peak b	Peak c	E_g	$E_g/1.15$	E_{ox-red}[35]
Cu[TPC]	0.74	1.66	2.39	1.0	0.85	0.96
Ag[TPC]	1.65	2.30	2.94	1.8	1.56	1.59
Au[TPC]	2.40	3.23	3.93	2.7	2.34	2.18

^{a}All values are in eV. The peak labels a−c are ordered simply according to increasing energy relative to the Fermi level and do not have any connotations relative to the nature of the unoccupied state involved.

while a lower temperature of 200 °C was used for Ag[TPC]. UPS and IPES experiments were performed on two distinct instruments. For IPES, the substrate was cut from a Si wafer covered by an amorphous carbon thin film. For UPS, an Au(111) film grown on a mica substrate was used. The cleanliness of the substrate and the thickness of the sample film were both probed by X-ray photoelectron spectroscopy and Auger electron spectroscopy. The film thickness used was large enough (several nm) so to avert problems arising from interface interaction or band bending.

IPES experiments were carried out in UHV at ~10^{-10} mbar base pressure. The measurements were performed in the isochromat mode, i.e., the incident electron kinetic energy was varied and emitted photons of fixed energy (9.7 eV) were collected by a band-pass photon analyzer consisting of a CaF$_2$ entrance window and a Geiger-Müller detector.[61] The incident electronic current was about 2 μA and the photon yield about 30−50 counts/s. The photon counts were normalized to the measured injected current. No significant sample degradation was observed when comparing the first and the last scan for each spectrum. The spectra were all referenced to the Fermi level measured on a clean Ta foil. The spectra were least-squares fitted with Gaussians with FWHM = 0.85 eV (in line with the energy resolution of the apparatus) along with an integral background.[72] UPS measurements were performed with He I (hν = 21.22 eV) radiation from a HIS 13 discharge lamp from Scienta Omicron. The emitted photoelectrons were counted using an R3000 analyzer equipped with a micro-channel plate detector. The resolution of the UPS measurements, determined from the width of the Fermi step on the metallic substrate, was 0.15 eV.

Figure 2 reports combined UPS-IPES-DFT spectra for the three M[TPC] thin films. On the filled-states side, essentially identical UPS spectra were measured, with very similar HOMO positions, consonant with similar electrochemical oxidation potentials for the three compounds.[35,62] The overall line shape was well reproduced by DFT, as expected for weakly interacting units in a molecular film.[63] On the other hand, IPES revealed major differences across the three molecules. From Cu through Ag to Au, a progressive shift to higher energies of the empty states was observed (Table 1), qualitatively mirroring the reduction potentials of the three complexes. Quantitatively, the solid-state band gap (E_g) as measured by UPS-IPES can be related to the electrochemical HOMO−LUMO gap (E_{ox-red}) with a normalization factor that accounts for different screening mechanisms (polarization) acting in the solid state vs in solution. As shown in Table 1, good agreement between the two energies was found with a normalization factor of 1.15.[58] A least-squares fit procedure revealed the presence of three low-energy states (see Gaussian curves beneath the spectra in Figure 2) that could be rationalized with the help of DFT results.

In the isolated molecules, the lowest-energy IPES feature can be assigned with a high degree of confidence from DFT calculations. Thus, the scalar-relativistic OLYP[64,65]-D3[66,67]/ZORA-STO-TZ2P method (which has been extensively tested by one of us[68−75]) yields gas-phase electron affinities[76−78] that closely track the energies of the lowest-energy IPES feature (Table 2). For Cu[TPC], the LUMO corresponds to an antibonding combination of the corrole π-HOMO and the formally empty Cu 3d$_{x2-y2}$ orbital, a consequence of the ligand noninnocence-driven saddled geometry of copper corroles (Figure 3). In the case of Ag[TPC], the saddling is much more muted so the corrole π-HOMO does not interact as much with the Ag 4d$_{x2-y2}$ orbital and the LUMO corresponds to essentially the latter orbital (Figure 3; note the significantly smaller amplitudes at the corrole *meso* positions relative to Cu[TPC]). A very different scenario holds for Au[TPC]: relativistic effects[79−81] raise the energy of the Au 5d$_{x2-y2}$ to such a degree that it corresponds to the LUMO+2, while the LUMO corresponds to a pure corrole-based π-orbital (Figure 3).

Accordingly, in each panel of Figure 2, the three lowest unoccupied Kohn−Sham states are color-coded: the green bar, corresponding to the state carrying M(d$_{x2-y2}$) character, moves to higher energy from Cu through Ag to Au. For Ag[TPC], the energy of the second IPES feature is very close to that of the first IPES feature of Au[TPC]. In light of the above discussion, it seems reasonable to assign this feature to a corrole-based LUMO. Indeed, the DFT-derived second electron affinities of both Cu[TPC] and Ag[TPC] are very close to the first electron affinity of Au[TPC] (Table 2). The assignment of the second IPES feature of Cu[TPC], however, remains somewhat uncertain. DFT calculations suggest that this feature should arise from an essentially corrole-based LUMO, but the energy

Table 2. Selected All-Electron OLYP-D3/ZORA-STO-TZ2P Energetics (eV)^a

Compound	IP$_1$ vertical	IP$_2$ vertical	EA$_1$ vertical	EA$_1$ adiabatic	EA$_2$ vertical	EA$_2$ adiabatic	$\Delta E_{HOMO-LUMO}$
Cu[TPC]	6.01 (^{2}B)	6.18 (^{2}A)	2.01 (^{2}B)	2.18 (^{2}B)	1.17 (^{2}A)	1.24 (^{2}A)	0.82
Ag[TPC]	5.96 (^{2}B)	6.28 (^{2}A)	1.38 (^{2}B)	1.61 (^{2}B)	1.28 (^{2}A)	1.35 (^{2}A)	1.19
Au[TPC]	6.01 (^{2}B)	6.35 (^{2}A)	1.14 (^{2}A)	1.22 (^{2}A)	0.77 (^{2}B)	1.14 (^{2}B)	1.75

^{a}The calculations were carried out with a scalar-relativistic ZORA (Zeroth Order Regular Approximation to the Dirac equation)[59] Hamiltonian, all-electron ZORA STO-TZ2P basis sets, fine integration grids and tight criteria for SCF and geometry optimization cycles, and C$_2$ point group symmetry, all as implemented in the ADF program system.[60] All IP and EA values were obtained via a ΔSCF procedure, i.e., as energy differences between initial and final states, with careful specification of electron occupancies in each irrep, where warranted. Note that a more positive electron affinity corresponds to a lower-energy LUMO. The HOMO-LUMO gaps ($\Delta E_{HOMO-LUMO}$) were obtained from Kohn-Sham orbital energies (see Figure 3).
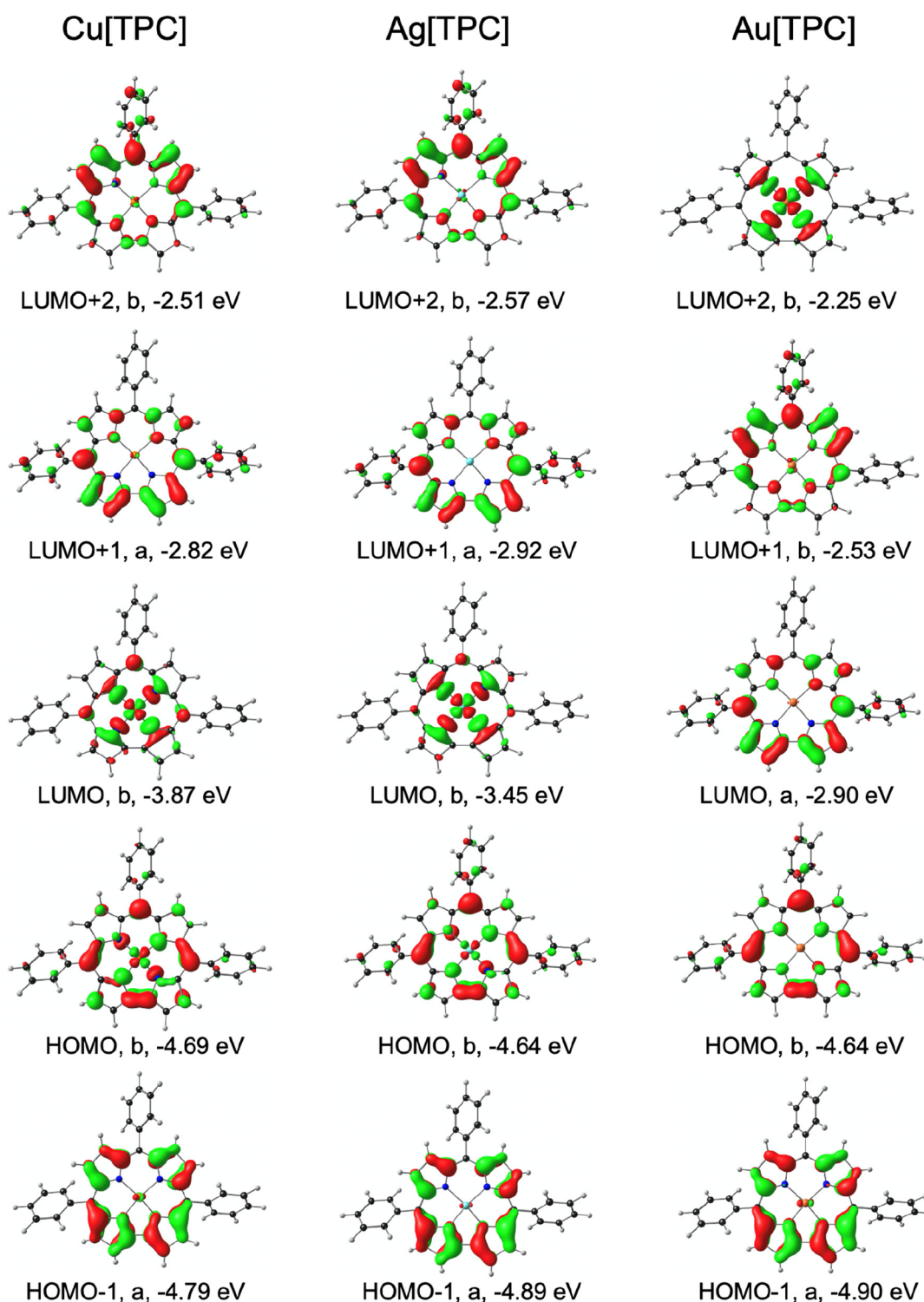
Figure 3. OLYP-D3/ZORA-STO-TZ2P frontier MOs of M[TPC], along with their C_2 irreps and Kohn–Sham orbital energies.

(1.66 eV) seems unduly lower than that of an analogous feature for Ag- and Au[TPC].

In summary, an IPES study of coinage metal triphenylcorroles has uncovered major differences in the energetics of the unoccupied states for the three metals. While the results nicely mirror those obtained from electrochemistry and DFT calculations, they also afford additional insight. Thus, in the case of Ag[TPC], IPES appears to have yielded unique experimental data on the energetics of the LUMO and LUMO

+1-derived anion states.[3−6] Overall, the IPES results are consistent with the electroactive nature of copper corroles, such as in dioxygen reduction and evolution processes, relative to gold corroles. The latter are of great interest as triplet photosensitizers, especially in photomedicine, in applications such as oxygen sensing and photodynamic therapy.[82−85] With continuing improvements in experimental methodology,[22] the day may not be far when IPES enjoys a significantly wider range of applications to metalloporphyrinoids and other

transition metal complexes, including catalysts and metallodrugs, and particularly inorganic polymers and other systems that are not readily studied with solution-phase techniques such as electrochemistry and optical spectroscopy.

ASSOCIATED CONTENT

Data Availability Statement

The data underlying this study are available in the published article and its Supporting Information.

Supporting Information

The Supporting Information is available free of charge at https://pubs.acs.org/doi/10.1021/acsorginorgau.4c00027.

Optimized DFT coordinates (PDF)

AUTHOR INFORMATION

Corresponding Authors

Luca Giovanelli − *Aix-Marseille Université, CNRS, IM2NP, Marseille 13397, France*; Email: luca.giovanelli@im2np.fr

Abhik Ghosh − *Department of Chemistry, UiT − The Arctic University of Norway, N-9037 Tromsø, Norway*; orcid.org/0000-0003-1161-6364; Email: abhik.ghosh@uit.no

Authors

Younal Ksari − *Aix-Marseille Université, CNRS, IM2NP, Marseille 13397, France*

Hela Mrezguia − *Aix-Marseille Université, CNRS, IM2NP, Marseille 13397, France*

Eric Salomon − *Aix-Marseille Université, CNRS, PIIM, Marseille 13397, France*; orcid.org/0000-0002-0567-7438

Marco Minissale − *Aix-Marseille Université, CNRS, PIIM, Marseille 13397, France*; orcid.org/0000-0001-6331-1402

Abraham B. Alemayehu − *Department of Chemistry, UiT − The Arctic University of Norway, N-9037 Tromsø, Norway*; orcid.org/0000-0003-0166-8937

Complete contact information is available at:
https://pubs.acs.org/10.1021/acsorginorgau.4c00027

Author Contributions

CRediT: **Luca Giovanelli** data curation, formal analysis, investigation, methodology, project administration, resources, supervision, visualization, writing-review & editing; **Younal Ksari** data curation, formal analysis, investigation, methodology; **Hela Mrezguia** investigation, methodology; **Eric Salomon** investigation, methodology; **Marco Minissale** investigation, methodology; **Abraham B. Alemayehu** investigation, methodology; **Abhik Ghosh** conceptualization, formal analysis, funding acquisition, investigation, project administration, resources, supervision, validation, writing-original draft, writing-review & editing.

Notes

The authors declare no competing financial interest.

ACKNOWLEDGMENTS

REFERENCES

(1) Di Natale, C.; Gros, C. P.; Paolesse, R. Corroles at work: A small macrocycle for great applications. *Chem. Soc. Rev.* **2022**, *51*, 1277−1335.

(2) Mahammed, A.; Gross, Z. Milestones and Most Recent Advances in Corrole's Science and Technology. *J. Am. Chem. Soc.* **2023**, *145*, 12429−12445.

(3) Levy, N.; Mahammed, A.; Kosa, M.; Major, D. T.; Gross, Z.; Elbaz, L. Metallocorroles as Nonprecious-Metal Catalysts for Oxygen Reduction. *Angew. Chem., Int. Ed.* **2015**, *54*, 14080−14084.

(4) Zhang, W.; Lai, W.; Cao, R. Energy-related small molecule activation reactions: oxygen reduction and hydrogen and oxygen evolution reactions catalyzed by porphyrin-and corrole-based systems. *Chem. Rev.* **2017**, *117*, 3717−3797.

(5) Lei, H.; Zhang, Q.; Liang, Z.; Guo, H.; Wang, Y.; Lv, H.; Li, X.; Zhang, W.; Apfel, U. P.; Cao, R. Metal-corrole-based porous organic polymers for electrocatalytic oxygen reduction and evolution reactions. *Angew. Chem., Int. Ed.* **2022**, *134*, No. e202201104.

(6) Thakur, M. S.; Singh, N.; Sharma, A.; Rana, R.; Syukor, A. A.; Naushad, M.; Kumar, S.; Kumar, M.; Singh, L. Metal coordinated macrocyclic complexes in different chemical transformations. *Coord. Chem. Rev.* **2022**, *471*, 214739.

(7) Teo, R. D.; Hwang, J. Y.; Termini, J.; Gross, Z.; Gray, H. B. Fighting cancer with corroles. *Chem. Rev.* **2017**, *117*, 2711−2729.

(8) Lemon, C. M. Corrole photochemistry. *Pure Appl. Chem.* **2020**, *92*, 1901−1919.

(9) Alemayehu, A. B.; Thomas, K. E.; Einrem, R. F.; Ghosh, A. The Story of 5d Metallocorroles: From Metal−Ligand Misfits to New Building Blocks for Cancer Phototherapeutics. *Acc. Chem. Res.* **2021**, *54*, 3095−3107.

(10) Zhan, X.; Kim, D.; Ullah, Z.; Lee, W.; Gross, Z.; Churchill, D. G. Photophysics of corroles and closely related systems for emergent solar energy, medicinal, and materials science applications. *Coord. Chem. Rev.* **2023**, *495*, 215363.

(11) Sharma, V. K.; Assaraf, Y. G.; Gross, Z. Hallmarks of anticancer and antimicrobial activities of corroles. *Drug Resistance Updates* **2023**, *67*, 100931.

(12) Thomas, K. E.; Alemayehu, A. B.; Conradie, J.; Beavers, C. M.; Ghosh, A. The Structural Chemistry of Metallocorroles: Combined X-Ray Crystallography and Quantum Chemistry Studies Afford Unique Insights. *Acc. Chem. Res.* **2012**, *45*, 1203−1214.

(13) Ghosh, A. Electronic structure of corrole derivatives: insights from molecular structures, spectroscopy, electrochemistry, and quantum chemical calculations. *Chem. Rev.* **2017**, *117*, 3798−3881.

(14) Ganguly, S.; Ghosh, A. Seven clues to ligand noninnocence: the metallocorrole paradigm. *Acc. Chem. Res.* **2019**, *52*, 2003−2014.

(15) Jørgensen, C. K. Differences between the four halide ligands, and discussion remarks on trigonal-bipyramidal complexes, on oxidation states, and on diagonal elements of one-electron energy. *Coord. Chem. Rev.* **1966**, *1*, 164−178.

(16) Kaim, W.; Schwederski, B. Non-innocent ligands in bioinorganic chemistry − An overview. *Coord. Chem. Rev.* **2010**, *254*, 1580−1588.

(17) Phung, Q. M.; Muchammad, Y.; Yanai, T.; Ghosh, A. A. DMRG/CASPT2 Investigation of Metallocorroles: Quantifying Ligand Noninnocence in Archetypal 3d and 4d Element Derivatives. *J. Am. Chem. Soc. Au* **2021**, *1*, 2303−2314.

(18) Phung, Q. M.; Nam, H. N.; Ghosh, A. Local Oxidation States in {FeNO}$^{6-8}$ Porphyrins: Insights from DMRG/CASSCF−CASPT2 Calculations. *Inorg. Chem.* **2023**, *62*, 20496−20505.

(19) Dose, V. Ultraviolet bremsstrahlung spectroscopy. *Prog. Surf. Sci.* **1983**, *13*, 225−283.

(20) Fauster, T.; Dose, V. Inverse photoemission spectroscopy. In *Chemistry and Physics of Solid Surfaces VI*; Vanselow, R., Howe, R., Eds.; Springer Series in Surface Sciences, Vol *5*; Springer,: Berlin, Heidelberg, 1986; pp 483−507. DOI: DOI: 10.1007/978-3-642-82727-3_18.

(21) Smith, N. V. Inverse photoemission. *Rep. Prog. Phys.* **1988**, *51*, 1227.

(22) Yoshida, H. Principle and application of low energy inverse photoemission spectroscopy: a new method for measuring unoccupied states of organic semiconductors. *J. Electron Spectrosc. Relat. Phenom.* **2015**, *204*, 116−124.

(23) Rao, C. N. R.; Basu, P. K.; Hegde, M. S. Systematic organic UV photoelectron spectroscopy. *Appl. Spectrosc. Rev.* **1979**, *15*, 1−193.

(24) Salaneck, W. R.; Lögdlund, M.; Fahlman, M.; Greczynski, G.; Kugler, T. The electronic structure of polymer−metal interfaces studied by ultraviolet photoelectron spectroscopy. *Mater. Sci. Eng. R Rep.* **2001**, *34*, 121−146.

(25) Ng, C. Y. Vacuum ultraviolet spectroscopy and chemistry by photoionization and photoelectron methods. *Annu. Rev. Phys. Chem.* **2002**, *53*, 101−140.

(26) Olthof, S. The impact of UV photoelectron spectroscopy on the field of organic optoelectronics—a retrospective. *Adv. Opt. Mater.* **2021**, *9*, 2100227.

(27) Zhou, X.; Yang, S.; Li, Q.; Bai, G.; Wang, C.; Han, C. Energy level measurement for organic semiconductors. *Phys. Chem. Chem. Phys.* **2024**, *26*, 2768−2779.

(28) Weaver, J. H. Electronic structures of C_{60}, C_{70} and the fullerides: Photoemission and inverse photoemission studies. *J. Phys. Chem. Solids* **1992**, *53*, 1433−1447.

(29) Sato, N.; Yoshida, H.; Tsutsumi, K. Unoccupied electronic states in phthalocyanine thin films studied by inverse photoemission spectroscopy. *Synth. Met.* **2003**, *133*, 673−674.

(30) Cook, P. L.; Yang, W.; Liu, X.; García-Lastra, J. M.; Rubio, A.; Himpsel, F. J. Unoccupied states in Cu and Zn octaethyl-porphyrin and phthalocyanine. *J. Chem. Phys.* **2011**, *134*, 204707.

(31) Classen, A.; Pöschel, R.; Di Filippo, G.; Fauster, T.; Malcıoğlu, O. B.; Bockstedte, M. Electronic structure of tetraphenylporphyrin layers on Ag (100). *Phys. Rev. B* **2017**, *95*, 115414.

(32) Giovanelli, L.; Lee, H. L.; Lacaze-Dufaure, C.; Koudia, M.; Clair, S.; Lin, Y. P.; Ksari, Y.; Themlin, J. M.; Abel, M.; Cafolla, A. A. Electronic structure of tetra(4-aminophenyl)porphyrin studied by photoemission, UV−Vis spectroscopy and density functional theory. *J. Electron Spectrosc. Relat. Phenom.* **2017**, *218*, 40−45.

(33) Soncini, C.; Bondino, F.; Magnano, E.; Bhardwaj, S.; Kumar, M.; Cepek, C.; Pedio, M. Electronic properties of carbon nanotubes as detected by photoemission and inverse photoemission. *Nanotechnology* **2021**, *32*, 105703.

(34) Sugie, A.; Han, W.; Shioya, N.; Hasegawa, T.; Yoshida, H. Structure-dependent electron affinities of perylene diimide-based acceptors. *J. Phys. Chem. C* **2020**, *124*, 9765−9773.

(35) Thomas, K. E.; Alemayehu, A. B.; Conradie, J.; Beavers, C.; Ghosh, A. Synthesis and Molecular Structure of Gold Triarylcorroles. *Inorg. Chem.* **2011**, *50*, 12844−12851.

(36) Ou, Z.; Shao, J.; Zhao, H.; Ohkubo, K.; Wasbotten, I. H.; Fukuzumi, S.; Ghosh, A.; Kadish, K. M. Spectroelectrochemical and ESR Studies of Highly Substituted Copper Corroles. *J. Porphyr. Phthalocyanines* **2004**, *8*, 1236−1247.

(37) Thomas, K. E.; Vazquez-Lima, H.; Fang, Y.; Song, Y.; Gagnon, K. J.; Beavers, C. M.; Kadish, K. M.; Ghosh, A. Ligand Noninnocence in Coinage Metal Corroles: A Silver Knife-Edge. *Chem.—Eur. J.* **2015**, *21*, 16839−16847.

(38) Wasbotten, I. H.; Wondimagegn, T.; Ghosh, A. Electronic Absorption, Resonance Raman, and Electrochemical Studies of Planar and Saddled Copper(III) *meso*-Triarylcorroles. Highly Substituent-Sensitive Soret Bands as a Distinctive Feature of High-Valent Transition Metal Corroles. *J. Am. Chem. Soc.* **2002**, *124*, 8104−8116.

(39) Brückner, C.; Briñas, R. P.; Bauer, J. A. K. X-ray Structure and Variable Temperature NMR Spectra of [*meso*-Triarylcorrolato]-copper(III). *Inorg. Chem.* **2003**, *42*, 4495−4497.

(40) Steene, E.; Dey, A.; Ghosh, A. *β*-Octafluorocorroles. *J. Am. Chem. Soc.* **2003**, *125*, 16300−16309.

(41) Bröring, M.; Brégier, F.; Tejero, E. C.; Hell, C.; Holthausen, M. C. Revisiting the Electronic Ground State of Copper Corroles. *Angew. Chem., Int. Ed.* **2007**, *46*, 445−448.

(42) Thomas, K. E.; Wasbotten, I. H.; Ghosh, A. Copper *β*-Octakis(trifluoromethyl)corroles: New Paradigms for Ligand Sub-stituent Effects in Transition Metal Complexes. *Inorg. Chem.* **2008**, *47*, 10469−10478.

(43) Alemayehu, A. B.; Gonzalez, E.; Hansen, L. K.; Ghosh, A. Copper Corroles Are Inherently Saddled. *Inorg. Chem.* **2009**, *48*, 7794−7799.

(44) Alemayehu, A. B.; Hansen, L. K.; Ghosh, A. Nonplanar, Noninnocent, and Chiral: A Strongly Saddled Metallocorrole. *Inorg. Chem.* **2010**, *49*, 7608−7610.

(45) Alemayehu, A. B.; Ghosh, A. Gold Corroles. *J. Porphyr. Phthalocyanines* **2011**, *15*, 106−110.

(46) Rabinovich, E.; Goldberg, I.; Gross, Z. Gold(I) and Gold(III) Corroles. *Chem.—Eur. J.* **2011**, *17*, 12294−12301.

(47) Thomas, K. E.; Beavers, C. M.; Ghosh, A. Molecular structure of a gold *β*-octakis (trifluoromethyl)-*meso*-triarylcorrole: an 85° difference in saddling dihedral relative to copper. *Mol. Phys.* **2012**, *110*, 2439−2444.

(48) Sinha, W.; Sommer, M. G.; Deibel, N.; Ehret, F.; Sarkar, B.; Kar, S. Silver Corrole Complexes: Unusual Oxidation States and Near-IR-Absorbing Dyes. *Chem.—Eur. J.* **2014**, *20*, 15920−15932.

(49) Capar, J.; Zonneveld, J.; Berg, S.; Isaksson, J.; Gagnon, K. J.; Thomas, K. E.; Ghosh, A. Demetalation of copper undecaarylcorroles: Molecular structures of a free-base undecaarylisocorrole and a gold undecaarylcorrole. *J. Inorg. Biochem.* **2016**, *162*, 146−153.

(50) Sinha, W.; Sommer, M. G.; van der Meer, M.; Plebst, S.; Sarkar, B.; Kar, S. Structural, electrochemical and spectroelectrochemical study on the geometric and electronic structures of [(corrolato)Au^{III}]^n (n = 0,+ 1,− 1) complexes. *Dalton Trans.* **2016**, *45*, 2914−2923.

(51) Sudhakar, K.; Mizrahi, A.; Kosa, M.; Fridman, N.; Tumanskii, B.; Saphier, M.; Gross, Z. Effect of selective CF_3 substitution on the physical and chemical properties of gold corroles. *Angew. Chem., Int. Ed.* **2017**, *56*, 9837−9841.

(52) Thomas, K. E.; Gagnon, K. J.; McCormick, L. J.; Ghosh, A. Molecular structure of gold 2, 3, 7, 8, 12, 13, 17, 18-octabromo-5, 10, 15-tris (4′-pentafluorosulfanylphenyl) corrole: Potential insights into the insolubility of gold octabromocorroles. *J. Porphyr. Phthalocyanines* **2018**, *22*, 596−601.

(53) Einrem, R. F.; Jonsson, E. T.; Teat, S. J.; Settineri, N. S.; Alemayehu, A. B.; Ghosh, A. Regioselective formylation of rhenium-oxo and gold corroles: substituent effects on optical spectra and redox potentials. *RSC Adv.* **2021**, *11*, 34086−34094.

(54) Fang, Y.; Ou, Z.; Kadish, K. M. Electrochemistry of Corroles in Nonaqueous Media. *Chem. Rev.* **2017**, *117*, 3377−3419.

(55) Sarangi, R.; Giles, L. J.; Thomas, K. E.; Ghosh, A. Ligand Noninnocence in Silver Corroles: A XANES Investigation. *Eur. J. Inorg. Chem.* **2016**, *2016*, 3225−3227.

(56) Lim, H.; Thomas, K. E.; Hedman, B.; Hodgson, K. O.; Ghosh, A.; Solomon, E. I. X-ray absorption spectroscopy as a probe of ligand noninnocence in metallocorroles: the case of copper corroles. *Inorg. Chem.* **2019**, *58*, 6722−6730.

(57) Krause, S.; Schöll, A.; Umbach, E. Determination of transport levels of inorganic semiconductors by ultraviolet and inverse photoemission. *Phys. Rev. B* **2015**, *91*, 195101.

(58) Sworakowski, J.; Lipiński, J.; Janus, K. On the reliability of determination of energies of HOMO and LUMO levels in organic semiconductors from electrochemical measurements. A simple picture based on the electrostatic model. *Org. Electron.* **2016**, *33*, 300−310.

(59) Van Lenthe, E. V.; Snijders, J. G.; Baerends, E. J. The zero-order regular approximation for relativistic effects: The effect of spin−orbit coupling in closed shell molecules. *J. Chem. Phys.* **1996**, *105*, 6505−6516.

(60) te Velde, G.; Bickelhaupt, F. M.; Baerends, E. J.; Fonseca Guerra, C.; van Gisbergen, S. J. A.; Snijders, J. G.; Ziegler, T. Chemistry with ADF. *J. Comput. Chem.* **2001**, *22*, 931−967.

(61) Forbeaux, I.; Themlin, J.-M.; Debever, J. M. Heteroepitaxial graphite on *6H*-SiC(0001): Interface formation through conduction-band electronic structure. *Phys. Rev. B* **1998**, *58*, 16396.

(62) Molecular orbital descriptions of coinage metal corroles have already been extensively reviewed.[12−14,35−37,55,56] For the benefit of the reader, however, we shall briefly comment on why the coinage

metal corroles exhibit similar HOMO energies (and oxidation potentials and UPS-derived first IPs), while the LUMO energies (and reduction potentials) are strongly metal-dependent. Unlike planar, innocent gold corroles,[45−52] copper corroles are *inherently saddled*,[38−44] which allows for part of the electron density of the corrole HOMO to flow into the empty d_{x2-y2} orbital of the formal Cu(III) center. This orbital interaction has mutually opposing effects that largely cancel each other out for the HOMO of Cu[TPC]: while saddling might be expected to mildly destabilize corrole π-MOs, the Cu(d_{x2-y2})-corrole(π) bonding interaction might be expected to be mildly stabilizing. That said, this orbital interaction is still rather weak so that the corresponding antibonding orbital, the LUMO of Cu[TPC], is only slightly above the HOMO in terms of orbital energy, which explains the low electron affinity, reduction potential, and HOMO−LUMO gap for the complex.

(63) Giovanelli, L.; Lee, H. L.; Lacaze-Dufaure, C.; Koudia, M.; Clair, S.; Lin, Y. P.; Ksari, Y.; Themlin, J. M.; Abel, M.; Cafolla, A. A. Electronic structure of tetra(4-aminophenyl)porphyrin studied by photoemission, UV-Vis spectroscopy and density functional theory. *J. Electron Spectrosc. Relat. Phenom.* **2017**, *218*, 40−45.

(64) Handy, N. C.; Cohen, A. Left-Right Correlation Energy. *J. Mol. Phys.* **2001**, *99*, 403−412.

(65) Lee, C.; Yang, W.; Parr, R. G. Development of the Colle-Salvetti correlation-energy formula into a functional of the electron density. *Phys. Rev. B* **1988**, *37*, 785−789.

(66) Grimme, S. Density Functional Theory with London Dispersion Corrections. *Wiley Interdiscip. Rev. Comput. Mol. Sci.* **2011**, *1*, 211−228.

(67) Grimme, S.; Antony, J.; Ehrlich, S.; Krieg, H. A Consistent and Accurate Ab Initio Parametrization of Density Functional Dispersion Correction (DFT-D) for the 94 Elements H-Pu. *J. Chem. Phys.* **2010**, *132*, 154104.

(68) Ghosh, A. Just how good is DFT? *J. Biol. Inorg. Chem.* **2006**, *11*, 671−673.

(69) Wasbotten, I.; Ghosh, A. Theoretical evidence favoring true iron (V)-oxo corrole and corrolazine intermediates. *Inorg. Chem.* **2006**, *45*, 4910−4913.

(70) Ghosh, A. Transition metal spin state energetics and noninnocent systems: challenges for DFT in the bioinorganic arena. *J. Biol. Inorg. Chem.* **2006**, *11*, 712−724.

(71) Conradie, J.; Ghosh, A. DFT calculations on the spin-crossover complex Fe (salen)(NO): a quest for the best functional. *J. Phys. Chem. B* **2007**, *111*, 12621−12624.

(72) Conradie, J.; Ghosh, A. Electronic structure of trigonal-planar transition-metal−imido complexes: spin-state energetics, spin-density profiles, and the remarkable performance of the OLYP functional. *J. Chem. Theory Comput.* **2007**, *3*, 689−702.

(73) Conradie, M. M.; Conradie, J.; Ghosh, A. Capturing the spin state diversity of iron (III)-aryl porphyrins: OLYP is better than TPSSh. *J. Inorg. Biochem.* **2011**, *105*, 84−91.

(74) Ghosh, A.; Conradie, J. Theoretical photoelectron spectroscopy of low-valent carbon species: a ∼ 6 eV range of ionization potentials among carbenes, ylides, and carbodiphosphoranes. *ACS Org. Inorg. Au* **2023**, *3*, 92−95.

(75) Ghosh, A.; Conradie, J. Theoretical Photoelectron Spectroscopy of Quadruple-Bonded Dimolybdenum(II,II) and Ditungsten(II,II) Paddlewheel Complexes: Performance of Common Density Functional Theory Methods. *ACS Omega* **2024**, *9*, 12237−12241.

(76) Ghosh, A.; Conradie, J. Porphyryne. *ACS Omega* **2022**, *7*, 40275−40278.

(77) Ghosh, A.; Conradie, J. The Perfluoro Cage Effect: A Search for Electron-Encapsulating Molecules. *ACS Omega* **2023**, *8*, 4972−4975.

(78) Torstensen, K.; Ghosh, A. From Diaminosilylenes to Silapyramidanes: Making Sense of the Stability of Divalent Silicon Compounds. *ACS Org. Inorg. Au* **2024**, *4*, 102−105.

(79) Ghosh, A.; Ruud, K. Relativity and the World of Molecules. *Am. Sci.* **2023**, *111*, 160−167.

(80) Das, A.; Das, U.; Das, R.; Das, A. K. Relativistic effects on the chemistry of heavier elements: why not given proper importance in chemistry education at the undergraduate and postgraduate level? *Chem. Teach. Int.* **2023**, *5*, 365−378.

(81) Pyykkö, P. Relativistic effects in chemistry: more common than you thought. *Annu. Rev. Phys. Chem.* **2012**, *63*, 45−64.

(82) Alemayehu, A. B.; Day, N. U.; Mani, T.; Rudine, A. B.; Thomas, K. E.; Gederaas, O. A.; Vinogradov, S. A.; Wamser, C. C.; Ghosh, A. Gold tris(carboxyphenyl)corroles as multifunctional materials: room temperature near-ir phosphorescence and applications to photodynamic therapy and dye-sensitized solar cells. *ACS Appl. Mater. Interfaces* **2016**, *8*, 18935−18942.

(83) Lemon, C. M.; Powers, D. C.; Brothers, P. J.; Nocera, D. G. Gold corroles as near-IR phosphors for oxygen sensing. *Inorg. Chem.* **2017**, *56*, 10991−10997.

(84) Zhan, X.; Lee, W.; Sudhakar, K.; Kim, D.; Mahammed, A.; Churchill, D. G.; Gross, Z. Solvent Effects on the Phosphorescence of Gold(III) Complexes Chelated by β-Multisubstituted Corroles. *Inorg. Chem.* **2021**, *60*, 8442−8446.

(85) Sahu, K.; Angeloni, S.; Conradie, J.; Villa, M.; Nayak, M.; Ghosh, A.; Ceroni, P.; Kar, S. NIR-emissive, singlet-oxygen-sensitizing gold tetra(thiocyano)corroles. *Dalton Trans* **2022**, *51*, 13236−13245.

G